ACS Photonics

Review

pubs.acs.org/journal/apchd5

Indefinite by Nature: From Ultraviolet to Terahertz

Jingbo Sun,[†,‡] Natalia M. Litchinitser,[‡] and Ji Zhou*[,†]

[†]State Kay Lab of New Ceramics and Fine Processing, School of Materials Science and Engineering, Tsinghua University, Beijing 100084, People's Republic of China

[‡]Electrical Engineering Department, University at Buffalo, The State University of New York, Buffalo, New York 14260, United States

Supporting Information

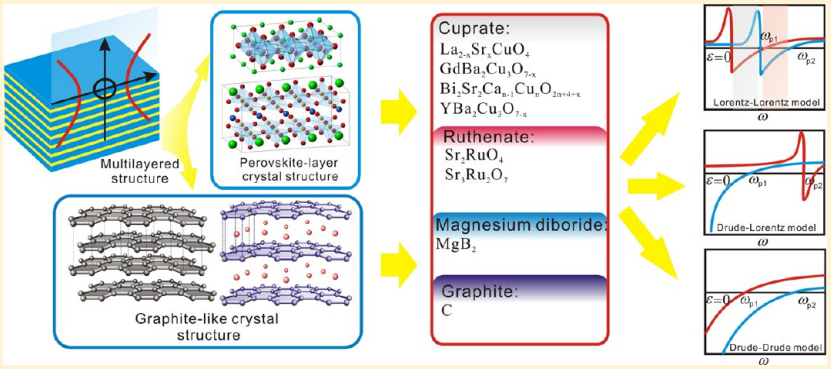

ABSTRACT: A class of strongly anisotropic materials having their principal elements of dielectric permittivity or magnetic permeability tensors of opposite signs, so-called indefinite or hyperbolic materials, has recently attracted significant attention. These materials enabled such novel properties and potential applications as all-angle negative refraction, high density of states, and imaging beyond the diffraction limit using a so-called hyperlens. While several studies identified a few examples of negative refractions in birefringent crystals existing in nature, the majority of optical materials with hyperbolic dispersion relations known to date are engineered composite materials, "metamaterials", such as metal-dielectric subwavelength multilayered structures or metal nanowires in a dielectric matrix. In this paper, we investigate naturally existing hyperbolic materials with indefinite permittivity for a range of frequencies from terahertz to ultraviolet. These include graphite, MgB_2, cuprate, and ruthenate. Spectroscopic ellipsometry is used to characterize the dielectric properties of graphite and MgB_2, and a fitting method based on reflectance spectra is used to determine the indefinite permittivity of the cuprate and ruthenate. Lastly, we discuss the mechanisms behind indefinite properties of these materials.

KEYWORDS: *indefinite property, hyperbolic materials, graphite, superconductor, ruthenate*

INTRODUCTION

Hyperbolic materials, also called indefinite materials, have attracted significant attention in recent years for their all-angle negative refraction with low loss.[1] The term indefinite material refers to a medium for which the permittivity and permeability tensor elements (along principal axes) are of opposite signs, resulting in a strong anisotropy, and as a result of such a strong anisotropy, the equifrequency contour (EFC) is hyperbolic.[2,3] Many novel and unique properties result from this hyperbolic EFC. First, hyperbolic materials give rise to an omnidirectional negative refraction for a certain polarization of the electromagnetic wave,[1,4−7] as shown in Figure 1a. As opposed to negative refraction in double-negative metamaterials that are composed of resonant meta-atoms and as any resonance-based structures are lossy, negative refraction in hyperbolic materials can be enabled by their unique dispersion relations and does not rely on any resonances and, therefore, is not accompanied by high losses.[1,5] Second, if the electromagnetic wave propagates in the direction of negative permittivity or permeability, the transverse wave vector k_x in Figure 1b will always be a real number for any k_z, implying that evanescent wave components would be converted into propagating waves that propagate without attenuation.[3,8] Since the evanescent wave components carry the information about subwavelength features of the object (source), hyperbolic materials make it possible to preserve such subwavelength information and to deliver it to the far field. This property forms the basis for a so-called hyperlens, enabling subwavelength imaging in the far field.[9−12] Next, hyperboloid EFC allowing propagating waves with extremely large wave vectors enables nanometer-scale three-dimensional cavities with a very large Q-value,[13,14] as shown in Figure 1c. Finally, the hyperbolic EFC is shown to greatly enhance the photonic density of states (PDOS) in a broad range of frequencies, paving the way for material-based PDOS engineering.[15−17] One of the potential applications of

Received: October 30, 2013
Published: February 14, 2014

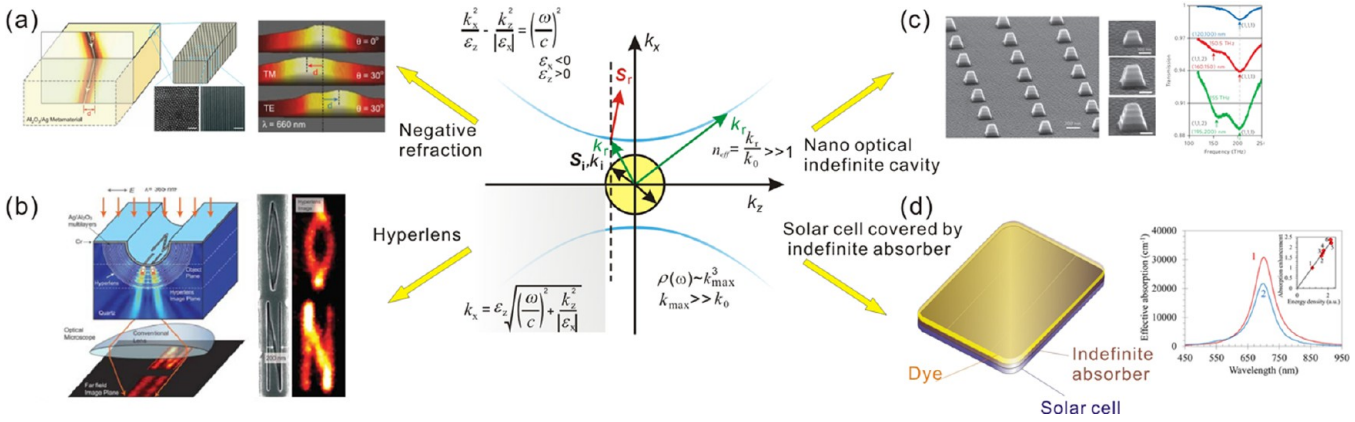

Figure 1. Novel properties and potential applications of the hyperbolic materials. (a) Negative refraction in the visible frequency range;[1] (b) hyperlens enabling subwavelength imaging in the far field;[10] (c) optical nanoscale cavity;[14] (d) hyperbolic material based absorber with high PDOS for high efficiency photovoltaic applications.[18]

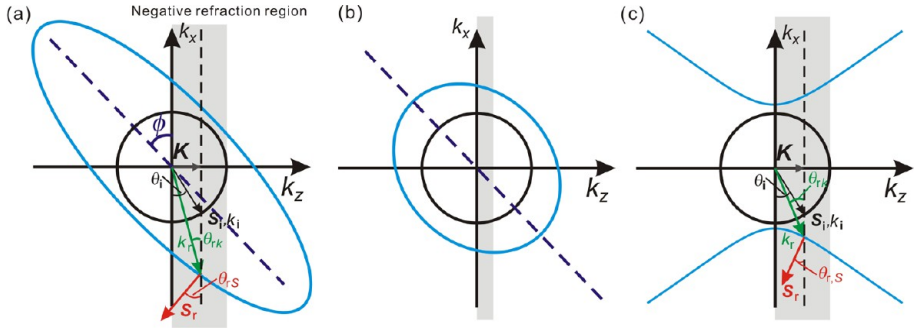

Figure 2. Relation of the material's anisotropy, its EFC, and the refraction behavior. (a) $\varepsilon_z \gg \varepsilon_x > 0$; (b) $\varepsilon_z > \varepsilon_x > 0$; (c) $\varepsilon_z > 0$, $\varepsilon_x < 0$. The black circles are the EFCs of the air, and the blue hyperbolas are the EFCs of the hyperbolic material. k_i and S_i are the incident wave vector and Poynting vector, respectively. k_r and S_r are the refractive wave vector and Poynting vector, respectively. The gray region describes the incident angles for which negative refraction may occur. For graphs (a) and (b), since all the anisotropic parameters are positive, the EFC is elliptical, as indicated by the blue circle. When the birefringent crystal is oriented obliquely with a certain angle ϕ, an incident wave with a certain incident angle θ_i may experience negative refraction. However, if the eccentricity of the ellipsoid is very small, the requirements of ϕ and θ_i are quite strict. For graph (c), incident light with any angle may refract negatively due to the hyperbolic EFC.

such increased PDOS is boosting the efficiency of solar cells by controlling the emission of the dye,[18] as shown in Figure 1d. In addition, the strong anisotropy of the hyperbolic material is likely to enable a novel, efficient polarization beam splitter,[19] beam steering applications,[20] and even a left-handed effect in the waveguide.[21]

In essence, negative refraction and its applications are shared by all anisotropic materials, but may be concealed if the anisotropy is not strong enough.[22,23] The dielectric properties of an anisotropic material are described by a tensor:

$$\tilde{\varepsilon} = \begin{pmatrix} \varepsilon_x & 0 & 0 \\ 0 & \varepsilon_y & 0 \\ 0 & 0 & \varepsilon_z \end{pmatrix} \quad (1)$$

where ε_x, ε_y, and ε_z are the components of dielectric permittivity along the x, y, and z directions, respectively. Considering the anisotropy in the zx-plane, the EFC can be written as

$$\frac{k_x^2}{\varepsilon_z} + \frac{k_z^2}{\varepsilon_x} = \frac{\omega^2}{c^2} \quad (2)$$

which is a quadratic function. The relative signs of ε_x and ε_z determine the type of EFC, e.g., an ellipse or a hyperbola. Figure 2 shows the relationship of the material's anisotropy, its EFC, and the refraction behavior. Materials with strong anisotropy ($\varepsilon_z \gg \varepsilon_x > 0$) and an elliptical EFC with a very large eccentricity, as shown in Figure 2a, have not been found yet, although in principle they could enable an all-angle negative refraction. Negative refraction was found in many natural anisotropic crystals with layered crystal structure, such as that in calcite,[24] YVO_4,[25,26] and liquid crystals,[27] as shown in Figure 3. However, comparing them to a hyperbolic media (Figure 2c), one finds that the anisotropies ($\varepsilon_z \approx \varepsilon_x > 0$) in these birefringent crystals are rather moderate. Their EFCs are ellipsoids of very small eccentricity, and therefore, the range of angles corresponding to negative refraction is very limited (Figure 2b). If the two permittivities have different signs ($\varepsilon_z > 0$, $\varepsilon_x < 0$), the material is a hyperbolic material and is characterized by a hyperbolic EFC, enabling the all-angle negative refraction, as shown in Figure 2c.

Often hyperbolic media are discussed in the context of metamaterials, which achieve novel properties that are not attainable in nature via designed artificial structures.[28−34] Well-studied structures for hyperbolic metamaterials are binary composites (metal/dielectric or two semiconductors), including those with multilayered structure,[6,12] cylindrical multilayered structure,[10,35] or metallic wire array.[1,5,11,36] In these structures, a negative element of the permittivity tensor was

dx.doi.org/10.1021/ph4000983 | ACS Photonics 2014, 1, 293−303

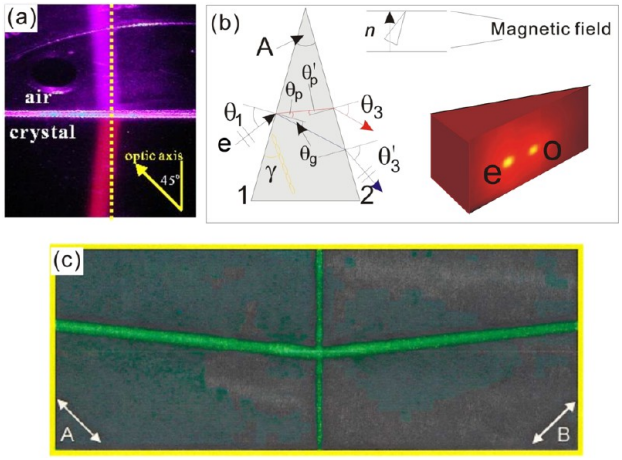

Figure 3. Examples of negative refraction in birefringent crystals: (a) calcite;[24] (b) liquid crystal;[27] (c) YVO_4.[25]

obtained along the conductive layers or the wires, while other permittivity tensor elements are always positive along the other perpendicular directions. Additionally, artificially made metamaterials, such as a fishnet structure, have also been shown to enable both indefinite permittivity and permeability.[37] Actually, some naturally occurring materials,[38] such as graphite or graphite-like material (MgB_2)[39,40] and crystal with perovskite-layer crystal structure (cuprate and ruthenate),[41−43] as shown in Figure 4, possess very similar structure to that of the layered

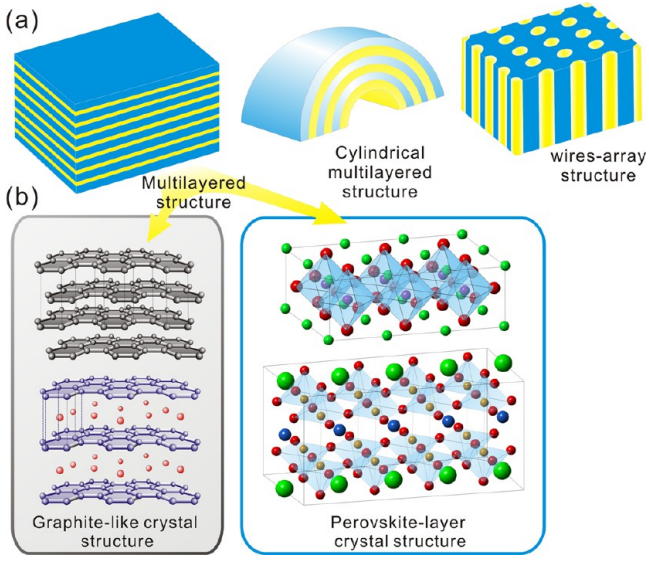

Figure 4. Typical structures of the intrinsic hyperbolic media. (a) Multilayered structure, cylindrical multilayered structure, and wire array structure.[1,5,6,10−12,35,36] (b) Common layered structures in different anisotropic crystals.

hyperbolic metamaterials, in spite of the different size scales of the layer. In contrast to the birefringent anisotropic structures, two-dimensional conductivity mechanisms of these materials make them act as conductors or superconductors in the macroscale. In the single-crystalline state, the dielectric property in the direction along the conductive layer is entirely different from those in the direction perpendicular to the layer, resulting in an indefinite dielectric tensor in the crystal. In this paper, we discuss naturally existing materials with strong dielectric anisotropy and analyze the feasibility to realize functional structures utilizing their indefinite dispersive properties. We propose a generalized phenomenological model for indefinite permittivity in natural materials, facilitating the development of new hyperbolic materials. We perform comprehensive theoretical and experimental studies and show that many existing natural materials, which scientists were familiar with for decades in different contexts, fall into the same large and important category: indefinite or hyperbolic materials that provide novel optical properties and functionalities such as negative refraction, high density of states, and subwavelength resolution.

GRAPHITE AS A HYPERBOLIC MATERIAL

Graphite is a semimetal with a uniaxial-layered crystalline structure. Carbon atoms of monocrystalline graphite are arranged in parallel graphene layers, forming a regular hexagonal network, as shown in Figure 5a. Each of the carbon atoms possesses one free π-electron with metallic conductance. Carbon atoms in layers form very strong covalent σ-bonds, while the layers are weakly held together through van der Waals interactions. Therefore, the conductance along the orientation normal to the graphene layer is dielectric. We use spectroscopic ellipsometry (WVASE, J. A. Woollam) to measure the anisotropic permittivity ε_o (permittivity along the graphite atom plane) and ε_e spectra (permittivity perpendicular to the graphite atom plane) of a highly ordered pyrolytic graphite (HOPG) sample in the range 240−400 nm, as shown in Figure 5b. These measurements indicate that the real part of the permittivity ε_{o1} is negative, whereas ε_{e1} is positive at ultraviolet (UV) wavelengths below 282 nm, leading to the indefinite permittivity of graphite in this wavelength range.[44]

If the crystal is oriented as shown in Figure 5c, the optical axis is parallel to both the sample surface and the plane of incidence so that the incident p-polarized light corresponds to the extraordinary wave and is modulated by the anisotropic dielectric constants of the crystal. In this case, the EFC of the uniaxial media is hyperbolic, as shown in Figure 1 and Figure 2c, and the Poynting vector S_r is parallel to the normal of the EFC. As a result, negative refraction is achieved from this hyperbolic dispersion, even though the phase velocity remains positive. Figure 5d shows the distribution of the magnetic field, confirming the predicted phenomenon of negative refraction at the interface.[44]

MAGNESIUM DIBORIDE AS A HYPERBOLIC MATERIAL

Magnesium diboride (MgB_2) is a graphite-like material possessing structural and electronic characteristics quite similar to graphite. The crystal structure of MgB_2 may be regarded as that of graphite intercalation compounds (GICs) with carbon replaced by boron (its neighbor in the periodic table, Figure 6a).[45] The Mg atoms are completely intercalated in the graphite-like boron planes. The anisotropic dielectric properties are determined by two distinct types of electronic bands: the strongly covalent almost two-dimensional (2D) bands derived from the hybridized sp_xp_y B orbitals and 3D bands made of p_z orbitals, as shown in Figure 6b,c.[46−49] In contrast to graphite, where the σ-bonding states are completely filled, providing a strong covalent bonding, the in-plane σ-bands of MgB_2 retain their 2D covalent character, but exhibit a metallic hole-type conductivity.[46] The coexistence of 2D metallic-type covalent band in-plane and 3D interlayer conducting bands is a peculiar

dx.doi.org/10.1021/ph4000983 | ACS Photonics 2014, 1, 293−303

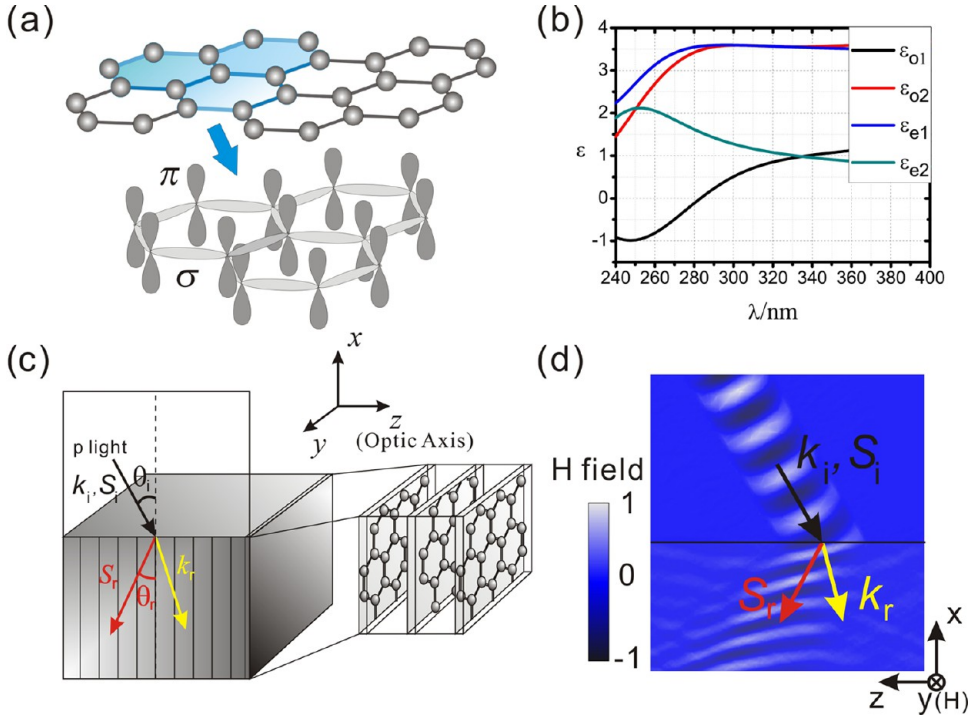

Figure 5. Indefinite properties of graphite.[44] (a) The crystal and bond (π, σ) states of graphite. (b) Spectral dependence of the anisotropic dielectric constants of graphite (subscript 1 denotes the real part and subscript 2 denotes the imaginary part); graphite is a hyperbolic medium in the wavelength range 240−280 nm. (c) The orientation of graphite leading to the negative refraction. (d) Simulation results of the negative refraction in graphite at 254 nm.

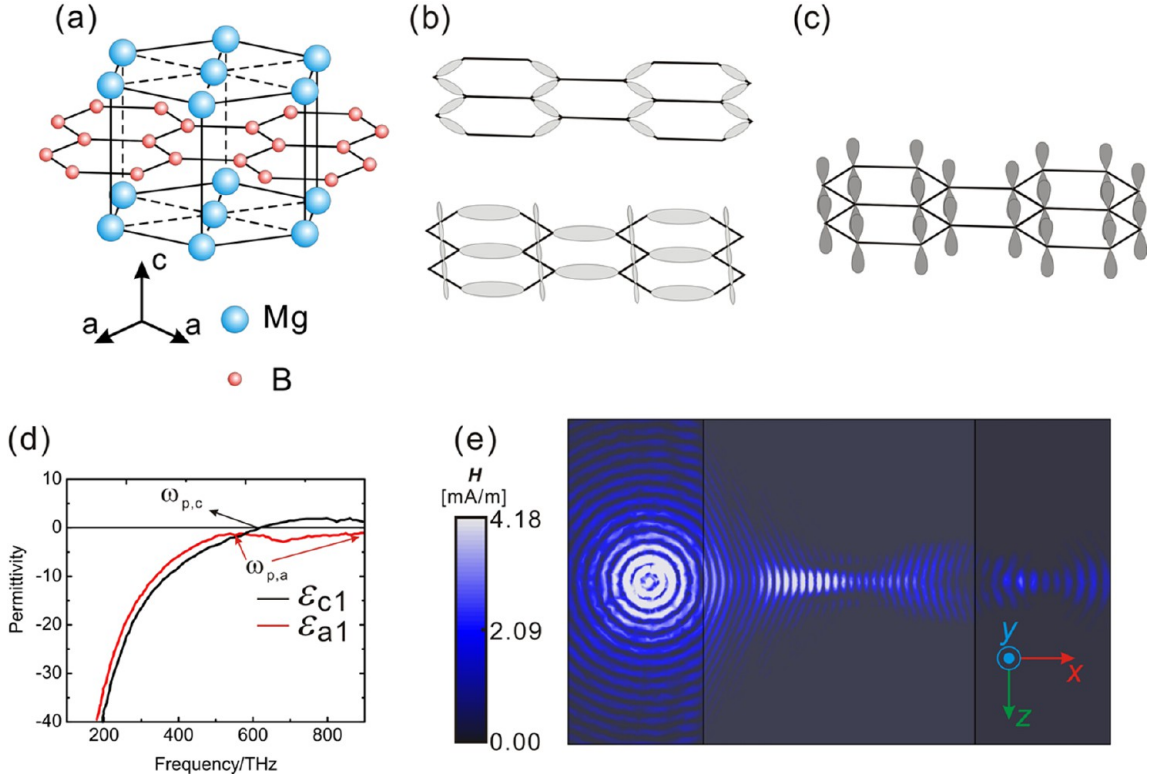

Figure 6. Indefinite property of the MgB_2. (a) The structure of MgB_2 contains graphite-like layers of B, which are intercalated by hexagonal close-packed layers of Mg. (b) σ-Bonding states at the Fermi level formed by the hybridized sp_xp_y B orbitals and (c) π-bands made of p_z B orbitals. (d) Spectral dependence of the anisotropic dielectric constants along the *a*- and *c*-axis in MgB_2 (subscript 1 denotes the real part of the permittivity).[48] The dielectric tensor is indefinite in the frequency range higher than the 627 THz. (e) Simulation results of a bulk MgB_2 working as a hyperlens at 702 THz.

dx.doi.org/10.1021/ph4000983 | ACS Photonics 2014, 1, 293−303

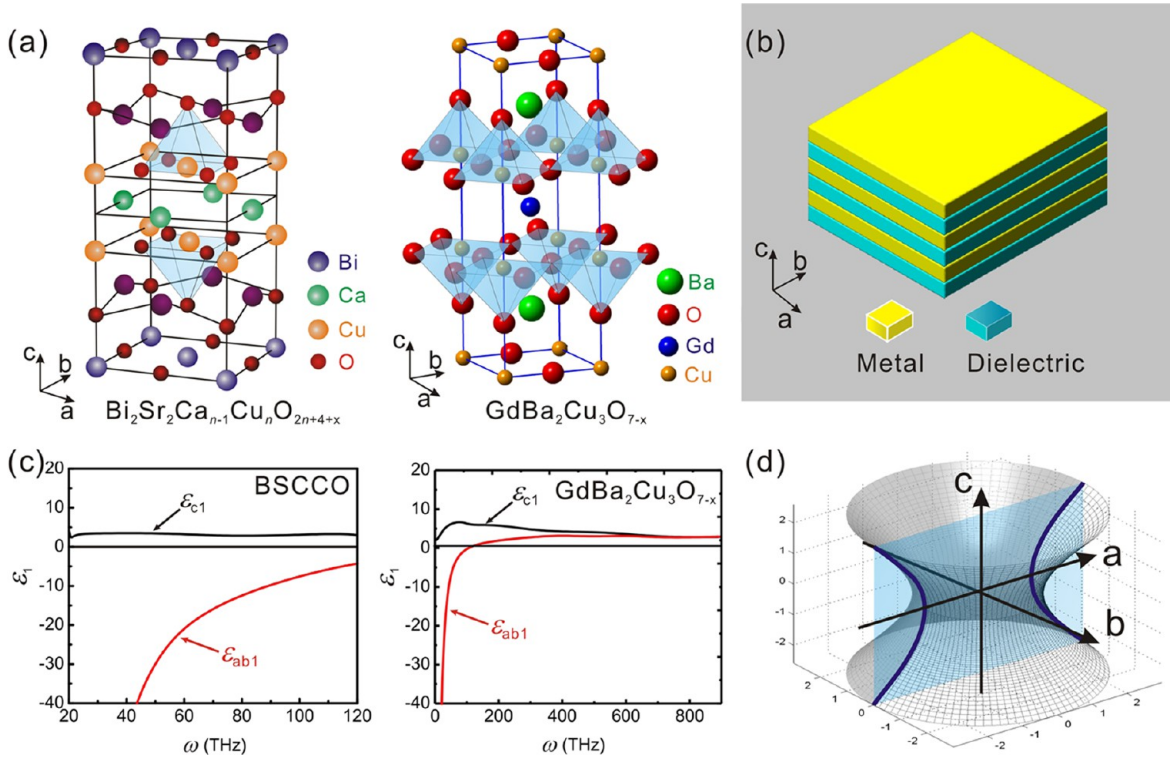

Figure 7. Indefinite permittivity of $Bi_2Sr_2Ca_{n-1}Cu_nO_{2n+4+x}$ (BSCCO) and $GdBa_2Cu_3O_{7-x}$. (a) Crystal structures of $Bi_2Sr_2Ca_{n-1}Cu_nO_{2n+4+x}$ and $GdBa_2Cu_3O_{7-x}$. (b) Effective model used to describe the dielectric properties of the two crystals. (c) Spectral dependence of the anisotropic dielectric constants along the *a*-, *b*-, and *c*-axis in $Bi_2Sr_2Ca_{n-1}Cu_nO_{2n+4+x}$ and $GdBa_2Cu_3O_{7-x}$ (subscript 1 denotes the real part of the permittivity). (d) Schematic EFC along different orientations of $YBa_2Cu_3O_{7-x}$ in the frequency range corresponding to indefinite permittivity. Because $\varepsilon_a < 0$, $\varepsilon_b < 0$, and $\varepsilon_c > 0$, the EFC is a hyperboloid of one sheet.

feature of MgB_2, which can be approximately described by the Drude model.[49] Figure 6d shows spectroscopic ellipsometry measurements of dielectric permittivities of MgB_2 between 627 and 900 THz at room temperature. These measurements indicate that MgB_2 is expected to exhibit a negative refraction for blue or violet light of a particular polarization. To confirm this prediction, we use Ansoft HFSS (High Frequency Structure Simulator) to do the numerical simulations of a MgB_2-based hyperlens at 702 THz, as shown in Figure 6e.

CUPRATES AS HYPERBOLIC MATERIALS

Cuprates are a class of well-studied superconductors with high critical temperature, T_c (above the boiling point of liquid nitrogen).[50−57] The relationship between the high-T_c mechanics and their anisotropic structures was studied extensively.[58−62] Usually, the hole band associated with the Cu−O planes results in a high conductance, which makes the cuprate act as a quasi-two-dimensional conductor.[63−68] However, there are still some differences among different cuprates. Below, we analyze in detail electronic structures of four main cuprate superconductors, $YBa_2Cu_3O_{7-x}$, $GdBa_2Cu_3O_{7-x}$, $La_{2-x}Sr_xCuO_4$, and $Bi_2Sr_2Ca_{n-1}Cu_nO_{2n+4+x}$, and reveal the indefinite dielectric properties in these materials.

It is noteworthy that $Bi_2Sr_2Ca_{n-1}Cu_nO_{2n+4+x}$ and $GdBa_2Cu_3O_{7-x}$ possess significantly different crystal structures, as illustrated in Figure 7a, but nevertheless very similar conducting mechanics. The conductance brought by the hole-band along the Cu−O plane is much higher than the hopping conductance along the *c*-axis, which results in a metallic permittivity of the Drude model in the *ab*-plane but a dielectric permittivity along the *c*-axis. As a result, both crystals can be described using an effective model consisting of alternative metal/dielectric layers as shown in Figure 7b. We use a retrieval method to retrieve the anisotropic dielectric constants between the *ab*-plane and the *c*-axis by fitting the reflection spectra obtained using Fourier transform infrared spectroscopy (FTIR) on $Bi_2Sr_2Ca_{n-1}Cu_nO_{2n+4+x}$[63] and Perkin-Elmer 16U spectrometer on $GdBa_2Cu_3O_{7-x}$[69] to a model for dielectric function. To obtain the permittivity, we use the Drude−Lorentz model with the form[70]

$$\varepsilon(\omega) = \varepsilon_\infty - \frac{{\omega_p}^2}{\omega^2 + i\Gamma\omega} + \sum_n \frac{{A_n}^2}{{\omega_n}^2 - \omega^2 - i\Gamma_n\omega} \quad (3)$$

where ε_∞ is the relativity permittivity as ω goes to infinity and the second term on the right-hand side is the usual Drude term with plasma frequency ω_p and damping frequency Γ. The terms in the summation correspond to optical-phonon modes (or, in principle, other excitations) with A_n, ω_n, and Γ_n giving the strength, plasma frequency, and damping frequency of the model, respectively. Therefore, dielectric dispersion is determined by the reflectance spectra fitting between the results computed by eq 3 and measured in the experiment (Figures S5 and S6 in the Supporting Information show the fitting results including reflectance spectra and complex dielectric constants spectra).

The fitting results shown in Figure 7c confirm that different components of dielectric permittivity have opposite signs, resulting in hyperbolic EFCs for both materials, as illustrated in Figure 7d.

Another example of a cuprate, yttrium barium copper oxide ($YBa_2Cu_3O_{7-x}$) that also possesses a layered structure is shown

dx.doi.org/10.1021/ph4000983 | ACS Photonics 2014, 1, 293−303

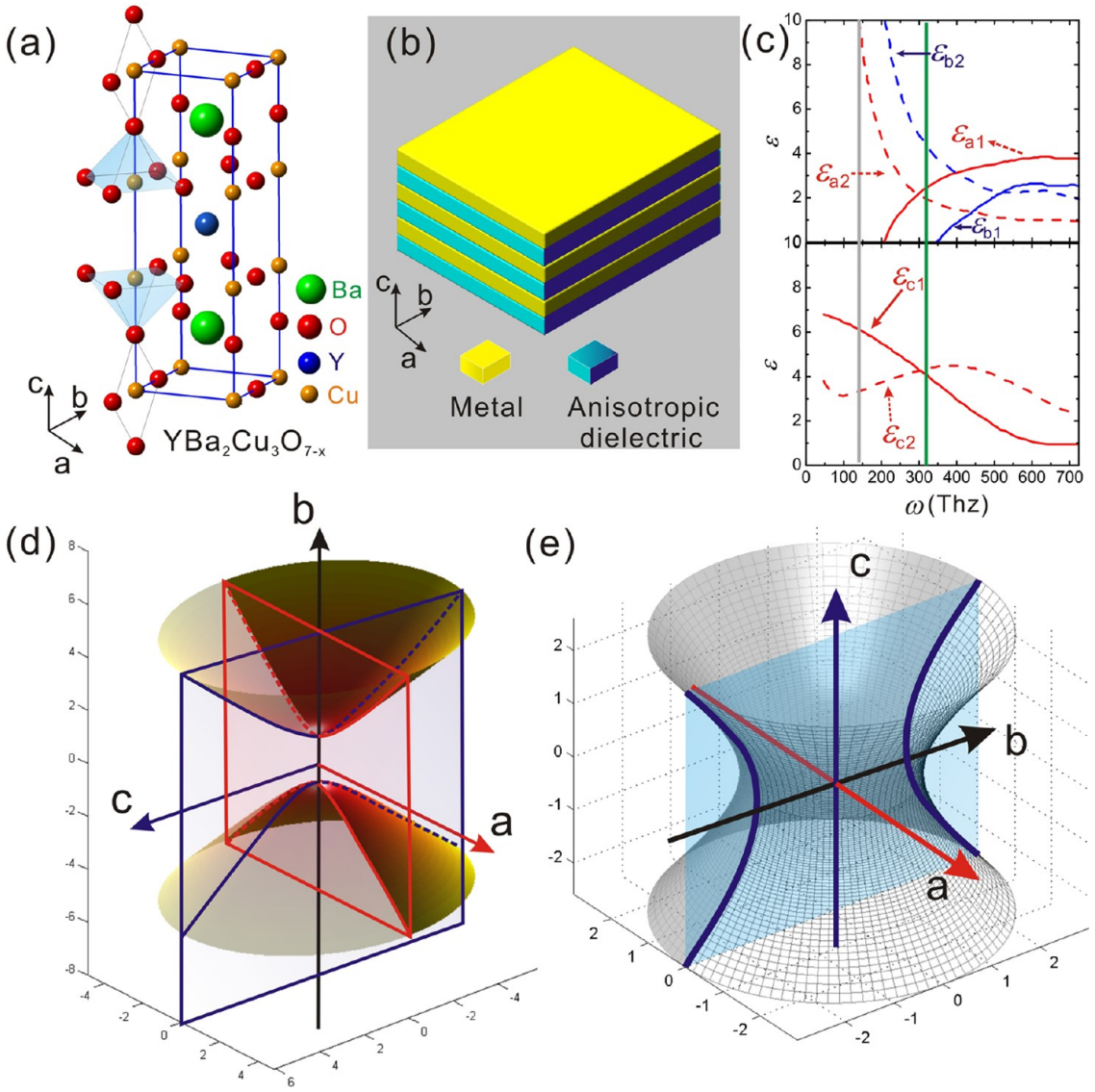

Figure 8. Indefinite permittivity of $YBa_2Cu_3O_{7-x}$. (a) The crystal structure of $YBa_2Cu_3O_{7-x}$. (b) The effective model used to describe the dielectric property of $YBa_2Cu_3O_{7-x}$. (c) Spectral dependence of the anisotropic dielectric constants of $YBa_2Cu_3O_{7-x}$ along three crystal orientations (subscript 1 denotes the real part and subscript 2 denotes the imaginary part);[67] the schematic EFC along different orientations of $YBa_2Cu_3O_{7-x}$ at the frequencies marked by green and gray lines in (c) are shown in (d) and (e). (d) Because $\varepsilon_a > 0$, $\varepsilon_b < 0$, and $\varepsilon_c > 0$ at the green line, the EFC is a hyperboloid of two sheets (the red curve and blue curve *ab*-plane and *bc*-plane, respectively). (e) At the frequency marked by the gray line, $\varepsilon_a < 0$, $\varepsilon_b < 0$, and $\varepsilon_c > 0$, and the EFC is a hyperboloid of one sheet with the *c*-axis as the symmetry axis.

in Figure 8a. The main conducting direction in this case is the *ab*-plane. However, due to the existence of the Cu−O chain along the *b* orientation, there is also an anisotropy between the *a* and *b* orientations.[65,66] We use an effective model of a multilayered structure composed of alternating dielectric layers and metal layers with arrays of ridges along the *b* direction (see Figure 8b) to describe the dielectric property. Previous work[67,71] shows that $YBa_2Cu_3O_{7-x}$ is a biaxial crystal with anisotropic permittivities along the three crystal orientations, ε_a, ε_b, and ε_c, as shown in Figure 8c, and become indefinite at the frequency range of <348 THz. As a result, its EFC is hyperbolic along three orientations in different frequency ranges, for example, at 340 THz along the *ab*- and *bc*-planes in Figure 8d and 120 THz along the *bc*-plane in Figure 8e.

Yet another interesting member of the cuprate family is $La_{1.92}Sr_{0.08}CuO_4$, which has the same structure as La_2CuO_4 but is doped heavily with Sr, as shown in Figure 9a, enabling a large hole-concentration. Despite the existence of the Cu−O plane, the reflectivity spectra of $La_{1.92}Sr_{0.08}CuO_4$ along the *c*-axis and the *ab*-plane resemble those of the insulators.[72] Using the fitting approach mentioned above (see Supplementary Figure S7), we obtain the anisotropic dielectric constants shown in Figure 9b. The principal features of the spectra in both directions look similar, composed by the superposition of several Lorentz oscillators, due to the infrared-active phonon resonances.[72] Many frequency ranges of indefinite permittivity are also produced by the overlapping resonance regions of the Lorentz model along two directions, marked by the gray and orange region in Figure 9b. Such series of Lorentz oscillators resemble the dielectric properties resulting from Mie scattering caused by subwavelengh particles. Therefore, we consider an array of rectangular particles to describe the several phonon oscillators, as illustrated in Figure 9c.

dx.doi.org/10.1021/ph4000983 | ACS Photonics 2014, 1, 293−303

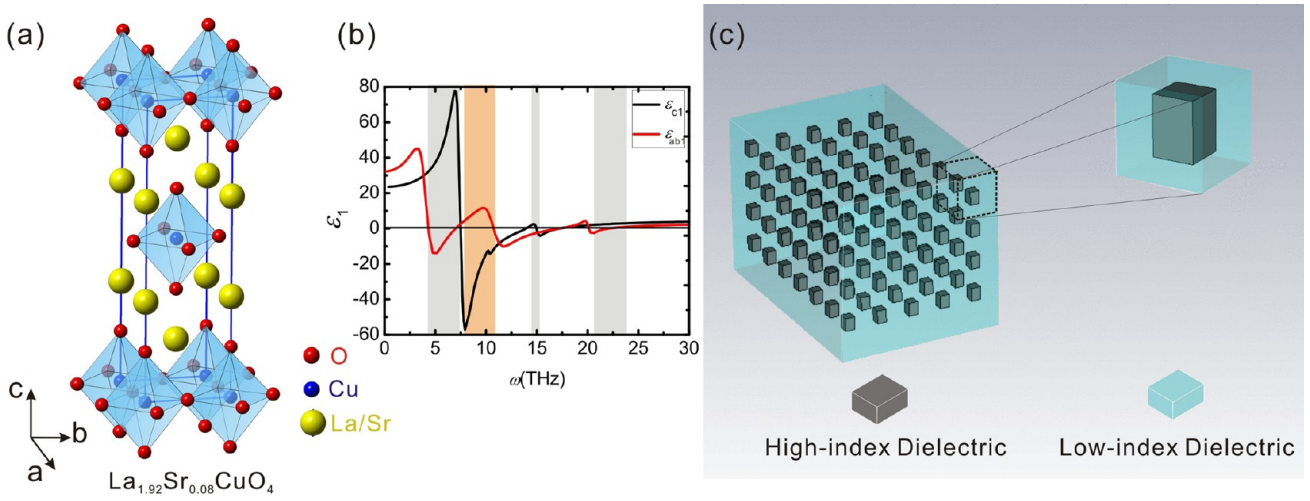

Figure 9. Indefinite permittivity of $La_{1.92}Sr_{0.08}CuO_4$. (a) The crystal structure of $La_{1.92}Sr_{0.08}CuO_4$. (b) Spectral dependence of the anisotropic dielectric constants of $La_{1.92}Sr_{0.08}CuO_4$ along two crystal orientations: the *ab*-plane and *c*-axis (subscript 1 denotes the real part of the permittivity). (c) The effective model used to describe the dielectric property of $La_{1.92}Sr_{0.08}CuO_4$. High refractive index particles embedded in a low refractive index matrix may result in a series of Lorentz resonances at the corresponding frequency, similar to the Mie resonances of different orders.

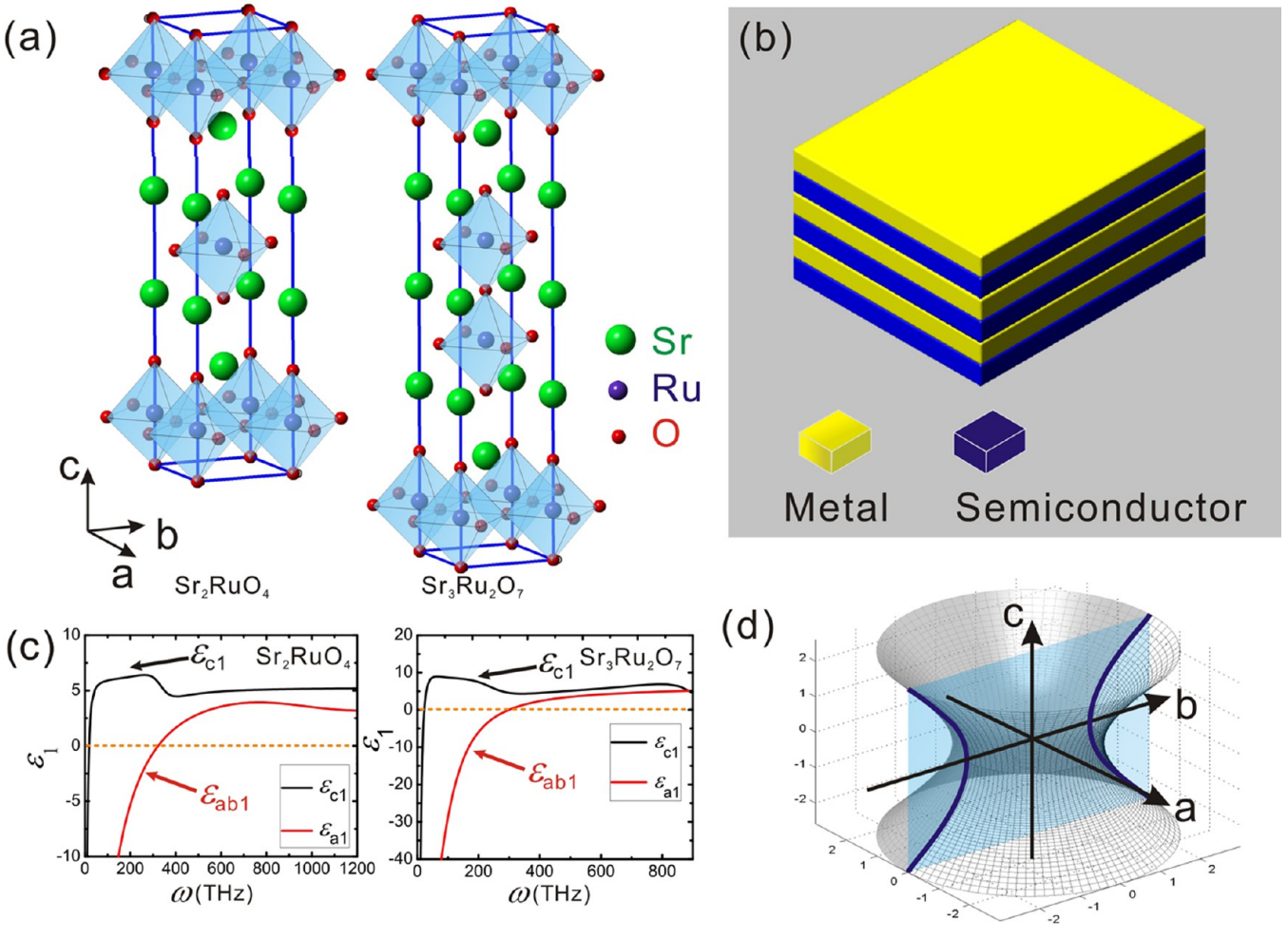

Figure 10. Indefinite permittivity of the ruthenate. (a) The crystal structures of Sr_2RuO_4 and $Sr_3Ru_2O_7$. (b) The effective model used to describe the dielectric property of Sr_2RuO_4 and $Sr_3Ru_2O_7$. (c) Spectral dependence of the anisotropic dielectric constants (*ab*-plane and *c*-axis) of the two composites (subscript 1 denotes the real part of the permittivity). The plasma frequencies of Sr_2RuO_4 are $\omega_{p,ab}$ = 19.2 THz, $\omega_{p,c}$ = 325.8 THz and the plasma frequencies of $Sr_3Ru_2O_7$ are $\omega_{p,ab}$ = 22 THz, $\omega_{p,c}$ =294 THz. (d) Schematic EFC along different orientations of the ruthenate at the frequency range with indefinite permittivity. Because $\varepsilon_a = \varepsilon_b = \varepsilon_{ab} < 0$, $\varepsilon_c > 0$, the EFC is a hyperboloid of one sheet.

dx.doi.org/10.1021/ph4000983 | ACS Photonics 2014, 1, 293−303

RUTHENATES AS HYPERBOLIC MATERIALS

Finally we consider another group of materials with perovskite-like layered crystalline structures. A Ruddlesden−Popper phase crystal, most generally described by a homologous series as $A_{n+1}B_nO_{3n+1}$, is a typical representative of this group.[73] Perovskite layers are formed by the corner-shared BO_6 octahedra in the *ab*-plane, and the number n determines the thickness of the octahedral layer. Ruthenate, $Sr_{n+1}Ru_nO_{3n+1}$, is one of the most important Ruddlesden−Popper phase materials, exhibiting electronic and magnetic properties covering a range from diamagnetic superconductor Sr_2RuO_4 (n = 1),[74,75] to paramagnetic conductor with antiferromagnetic (AFM) correlation (n = 2),[76] to ferromagnetic (FM) metal (n = 3, ∞).[77] Yet another, previously overlooked peculiar property of ruthenate is the anisotropic reflection property of Sr_2RuO_4 (n = 1) and $Sr_3Ru_2O_7$ (n = 2), which is likely to be attributed to its indefinite permittivity.

The crystal structures of Sr_2RuO_4 and $Sr_3Ru_2O_7$ are shown in Figure 10a, having one layer RuO_6 octahedra thick and two layers RuO_6 octahedra thick, respectively. Despite a similar perovskite structure to the cuprate, both of the anisotropic reflectance spectra in the *ab*-plane and along the *c*-axis of the ruthenate are metallic.[78,79] Therefore, we were able to fit their dielectric permittivities using Drude models with two different plasma frequencies, as shown in Figure 10c. This is quite different from the cuprate with a dielectric property along the *c*-axis in Figure 7c and Figure 8c. Indefinite permittivity and a hyperbolic EFC can be achieved at the frequency range between the two plasma frequencies, as illustrated in Figure 10d. Figure S9 in the Supporting Information shows fitting results including reflectance spectra and complex dielectric constants spectra.

DISCUSSION

On the basis of the results above, we put forward the following generalized model for the mechanisms of the intrinsic indefinite permittivity in several families of naturally existing layered structures. Three types of mechanisms were identified, Drude−Drude type, Drude−Lorentz type, and Lorentz−Lorentz type, as shown in Figure 11.

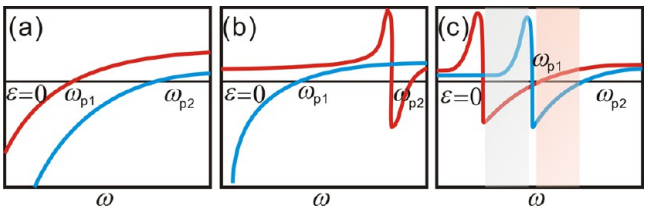

Figure 11. Basic mechanisms of the intrinsic hyperbolic medium: (a) Drude−Drude type; (b) Drude−Lorentz type; and (c) Lorentz−Lorentz type.

For the Drude−Drude type, conductance along all orientations of the crystal in the incident plane is metallic but with different conductive ability. Thus, both of the dielectric spectra can be described by Drude models with two different plasma frequencies (ω_{p1} and ω_{p2}); see Figure 11a. As a result, the permittivity tensor in the frequency range between ω_{p1} and ω_{p2} is indefinite, leading to the negative refraction of the incident light waves. Crystals of MgB_2, Sr_2RuO_4, and $Sr_3Ru_2O_7$ belong to this type.

For the Drude−Lorentz type, the conductances along different orientations are quite different from each other. One is metallic and the other one is of an insulator, resulting in a Drude dispersion and Lorentz dispersion with possible resonances at high frequency, respectively. Consequently, there are indefinite permittivities at the frequency range below the plasma frequency of the Drude mode; see Figure 11b. Crystals of $GdBa_2Cu_3O_{7-x}$ and $Bi_2Sr_2CaCu_2O_{8+x}$ belong to this type.

For the Lorentz−Lorentz type, conductance properties along all orientations are dielectric. Possibly due to the lattice vibration or some other oscillators, there will be several Lorentz resonances appearing in the dielectric spectrum along each direction; see Figure 11c. Therefore, it turns out that several frequency ranges of indefinite permittivity may be produced by the overlapping of the resonant regions from one Lorentz model in one direction and nonresonant region from the other Lorentz model in the perpendicular direction, such as the phenomenon in $La_{1.92}Sr_{0.08}CuO_4$.

The indefinite mechanism in $YBa_2Cu_3O_{7-x}$ crystal along different orientations can be classified as two types. Anisotropy between the *ab*-plane and *c*-axis results in the indefinite permittivity of a Drude−Lorentz type, for the metallic behavior in the *ab*-plane and the dielectric behavior along the *c*-axis. Moreover, the anisotropy in the *ab*-plane itself caused by the Cu−O chain along the *b*-axis results in the indefinite permittivity between the *a*- and *b*-axis of a Drude−Drude type. Therefore, such a crystal may contain two or more types of indefinite permittivity along different orientations.

Finally, we prove that the above phenomenological generalized model indeed accurately describes the underlying physical mechanism behind the indefinite properties of materials. Let us consider in detail the indefinite properties of graphite. As we discussed above, for the electric field polarized in the basal plane, π-electrons that arise from each atom can move freely within the two-dimensional graphene layer, which accounts for a negative ε_o below approximately 0.9 eV (or 1.4 μm). Thus, ε_o can be expressed as a Drude model with a plasma frequency of approximately 0.9 eV.[80] For photon energies above 0.9 eV, the interband transition ($\sigma-\pi$) along with the intraband transition contributes to ε_o.[81] The intraband part of the dielectric function is described by the Drude model, whereas the other part can be described using a modified Lorentz model.[82] At a photon energy of around 5 eV (240 nm), the hybrid resonance involving both π-and σ-electrons results in a negative ε_o with a plasma frequency of about 7 eV.[81] For the electric field polarized perpendicular to the basal plane, the transitions between the π-bands are forbidden,[83] and ε_e is always positive. Therefore, the indefinite permittivity at the range below 0.9 eV belongs to the Drude−Lorentz type, while the one discussed in this paper belongs to a "Drude combined with Lorentz"−Lorentz type. Considering that the negative ε_o below 0.9 eV has a very large imaginary part,[80,84] which results in a high loss, the spectral region around 5 eV (248 nm) is intended to be used as the operating band. Therefore, a crystal may contain various types of indefinite permittivity at different frequency ranges in the same orientation. A recently reported paper shows that a triglycine sulfate single crystal also exhibits the Drude−Lorentz type indefinite dielectric property in the THz range and the Drude−Drude type indefinite dielectric property in the far-infrared range.[85]

Another example of the natural indefinite material is α-Al_2O_3, which exhibits an indefinite permittivity in the infrared range

dx.doi.org/10.1021/ph4000983 | ACS Photonics 2014, 1, 293−303

due to the polar lattice vibrations in different directions, parallel or perpendicular to the crystal axis of anisotropic crystals.[86] Despite its rhombohedral crystal structure that is common in insulated crystals, the indefinite permittivity of the α-Al_2O_3 crystal can be described by the Lorentz−Lorentz model. This also shows that the universal compatibility of our model can also involve indefinite crystals with nonlayered crystal structure types.

It is noteworthy that hyperbolic materials are not limited to those with indefinite dielectric properties. It is also possible to find indefinite magnetic properties in naturally existing materials. Typical magnetic materials are ferrite materials, which may exhibit indefinite permeability from the radio to microwave range.[87,88] Moreover, recent studies on ultrafast manipulation of magnetic states in perovskite transition metal oxides indicate a possibility of achieving high-frequency magnetism.[89]

Besides the indefinite properties, another type of anisotropy with nonzero off-diagonal elements in eq 1 could also be very useful. Indeed, such materials, referred to as chiral materials, were first discussed to realize negative refraction.[90,91] Moreover, recently they were shown to greatly enhance repulsive optical gradient force.[92] Therefore, understanding the mechanisms behind crystals' resonances opens the possibility of finding such chiral materials in nature.

CONCLUSIONS AND OUTLOOK

In conclusion, although the optics of hyperbolic materials is still a relatively young research field, in addition to fascinating physics underlying the unique properties of hyperbolic materials, this field already proved its great potential for a number of applications. While first discussed in detail in the context of metamaterials, it turns out that indefinite properties also appear in natural crystals. Not underestimating the design flexibility provided by the metamaterial approach, we should highlight that the availability of naturally existing hyperbolic materials offers several advantages, being the availability of large samples, elimination of the need for often expensive and time-consuming nanofabrication, and elimination of losses associated with fabrication imperfections.

In this paper, we investigated the indefinite dielectric properties in several kinds of layer structured crystals: graphite, MgB_2, cuprates, and ruthenates. The two-dimensional conductivity mechanisms of the parallel atomic plane are responsible for the indefinite permittivity of these layered structure crystals. Indefinite permittivity in single crystals of graphite and MgB_2 was demonstrated by ellipsometry measurements in the visible−UV range, and electromagnetic parameter retrieval from the reflectance spectra showed the indefinite permittivity in cuprate and ruthenate in the infrared to THz range. The indefinite properties of these crystals cover the range from THz to UV frequencies (the entire list of the eight materials' indefinite frequency range can be found as Supplementary Table S1), opening nearly unlimited possibilities for device applications. As a homogeneous material, intrinsic hyperbolic materials hold the advantage of no wave scattering caused by the inner structures in the artificially engineered materials and eliminating the need for complicated design and fine fabrication techniques inevitable in manmade materials, therefore opening a new route to practical applications of their unique properties.

By summarizing the mechanisms for the dielectric anisotropy, we classified the intrinsic indefinite properties of crystals into three types. More complicated indefinite dielectric dispersions, such as in the crystals of graphite, $YBa_2Cu_3O_{7-x}$, can be analyzed by combining the three basic types. Other crystals such as Al_2O_3, despite having of no standard layered structure, can also be described by these generalized models. Layered crystals discussed in this paper containing a 2D conducting system can be approximately described by the multilayered effective model, while the crystals with a 1D conducting structure, following the model of a wire array, are still under exploration. Further understanding of the basic indefinite dielectric mechanism paves the way for the exploration of other intrinsic hyperbolic materials and their potential applications.

METHODS

The materials we report here are studied by two methods. One is the direct characterization by an ellipsometer, applied to a graphite crystal and MgB_2 crystal. The ellipsometer may show the anisotropic dielectric spectra along different crystal orientations directly and then determine the indefinite frequency band. The other method is to compute the anisotropic permittivity by fitting the modeling reflectance to the experimental reflectance, applied to the cuprates and ruthenates. The detailed ellipsometry measurement and fitting method can be found in the Supporting Information.

ASSOCIATED CONTENT

Supporting Information

Detailed information on the ellipsometry measurements, fitting methods, and a summary of the indefinite wavelength or frequency ranges for materials studied in this paper is available free of charge via the Internet at http://pubs.acs.org.

AUTHOR INFORMATION

Corresponding Author

*E-mail: zhouji@mail.tsinghua.edu.cn.

Notes

The authors declare no competing financial interest.

ACKNOWLEDGMENTS

This work was supported by the National Natural Science Foundation of China under Grant Nos. 51032003 and 11274198 and National High Technology Research and Development Program of China under Grant No. 2012AA030403. N.L. and J.S. acknowledge support from the U.S. Army Research Office under the award W911NF-11-1-0333 and the U.S. National Science Foundation under the award 1231852.

REFERENCES

(1) Yao, J.; Liu, Z. W.; Liu, Y. M.; Wang, Y.; Sun, C.; Bartal, G.; Stacy, A. M.; Zhang, X. Optical negative refraction in bulk metamaterials of nanowires. *Science* **2008**, *321*, 930.

(2) Smith, D. R; Schurig, D. Electromagnetic wave propagation in media with indefinite permittivity and permeability tensors. *Phys. Rev. Lett.* **2003**, *90*, 077405−077409.

(3) Fang, A.; Koschny, T.; Soukoulis, C. M. Optical anisotropic metamaterials. Negative refraction and focusing. *Phys. Rev. B* **2009**, *79*, 245127−245133.

(4) Lindell, I. V.; Tretyakov, S. A.; Nikosklnen, K. I.; Ilvoene, S. BW media-media with negative parameters, capable of supporting backward waves. *Microwave Opt. Technol. Lett.* **2001**, *31*, 129−133.

(5) Liu, Y. M.; Bartal, G.; Zhang, X. All-angle negative refraction and imaging in a bulk medium made of metallic nanowires in the visible region. *Opt. Exp.* **2008**, *16*, 15439−15448.
(6) Hoffman, A. J.; Alekseyev, L.; Howard, S. S.; Franz, K. J.; Wasserman, D.; Podolskiy, V. A.; Narimanov, E. E.; Sivco, D. L.; Gmachl, C. Negative refraction in semiconductor metamaterials. *Nat. Mater.* **2007**, *6*, 946−950.
(7) Smith, D. R.; Schurig, D.; Mock, J. J.; Kolinko, P.; Rye, P. Partial focusing of radiation by a slab of indefinite media. *Appl. Phys. Lett.* **2004**, *84*, 2244−2246.
(8) Jacob, Z.; Alekseyev, L. V.; Narimanov, E. Optical hyperlens, far-field imaging beyond the diffraction limit. *Opt. Exp.* **2006**, *14*, 8247−8256.
(9) Lee, H.; Liu, Z. W.; Xiong, Y.; Sun, C.; Zhang, X. Development of optical hyperlens for imaging below the diffraction limit. *Opt. Exp.* **2007**, *15*, 15886−15891.
(10) Liu, Z. W.; Lee, H.; Xiong, Y.; Sun, C.; Zhang, X. Far-field optical hyperlens magnifying sub-diffraction-limited objects. *Science* **2007**, *315*, 1686.
(11) Lu, W. T.; Sridhar, S. Superlens imaging theory for anisotropic nanostructured metamaterials with broadband all-angle negative refraction. *Phys. Rev. B* **2008**, *77*, 233101−233104.
(12) Xiong, Y.; Liu, Z.; Sun, C.; Zhang, X. Two-dimensional imaging by far-field superlens at visible wavelengths. *Nano Lett.* **2007**, *7*, 3360−3365.
(13) Yao, J.; Yang, X.; Yin, X.; Bartal, G.; Zhang, X. Three-dimensional nanometer-scale optical cavities of indefinite medium. *Proc. Natl. Acad. Sci. U.S.A.* **2011**, *108*, 11327−11331.
(14) Yang, X.; Yao, J.; Rho, J.; Yin, X.; Zhang, X. Experimental realization of three-dimensional indefinite cavities at the nanoscale with anomalous scaling laws. *Nat. Photonics* **2012**, *6*, 450−454.
(15) Jacob, Z.; Kim, J. -Y.; Naik, G. V.; Boltasseva, A.; Narimanov, E. E.; Shalaev, V. M. Engineering photonic density of states using metamaterials. *Appl. Phys. B: Laser Opt.* **2010**, *100*, 215−218.
(16) Noginov, M. A.; Li, H.; Barnakov, Y. A.; Dryden, D.; Nataraj, G.; Zhu, G.; Bonner, C. E.; Mayy, M.; Jacob, Z.; Narimanov, E. E. Controlling spontaneous emission with metamaterials. *Opt. Lett.* **2010**, *35*, 1863−1865.
(17) Tumkur, T. U.; Kitur, J. K.; Chu, B.; Gu, L.; Podolskiv, V. A.; Narimanov, E. E.; Noginov, M. A. Control of reflectance and transmittance in scattering and curvilinear hyperbolic metamaterials. *Appl. Phys. Lett.* **2012**, *101*, 091105−091109.
(18) Tumkur, T. U.; Gu, L.; Kitur, J. K.; Narimanov, E. E.; Noginov, M. A. Control of absorption with hyperbolic metamaterials. *Appl. Phys. Lett.* **2012**, *100*, 161103−161106.
(19) Sun, J.; Liu, L.; Dong, G.; Zhou, J. Efficient polarization beam splitter based on an indefinite medium. *J. Electro Magn. Wave Appl.* **2012**, *26*, 1423−1431.
(20) Sun, J.; Sun, T.; Li, B.; Chan, H. L. W.; Zhou, J.; Wang, Y. Controlling the electromagnetic field by indefinite media with extremely strong anisotropy. *Prog. Electromagn. Res.-Pier.* **2012**, *130*, 513−524.
(21) Podolskiy, V. A.; Narimanov, E. E. Strongly anisotropic waveguide as a nonmagnetic left-handed system. *Phys. Rev. B* **2005**, *71*, 201101.
(22) Zhang, W. Q.; Yang, F. Negative refraction at various crystal interfaces. *Opt. Commun.* **2008**, *28*, 3081−3086.
(23) Brazhe, R. A.; Meftakhutdinov, R. M. Negative optical refraction in crystals with strong birefringence. *Tech. Phys.* **2007**, *52*, 793−795.
(24) Yau, F. H.; Liu, J. P.; Ke, B.; Kuo, C. H.; Ye, Z. Comment on "Total negative refraction in real crystals for ballistic electrons and light". *ArXiv: cond-mat*, 2003, 0312125.
(25) Zhang, Y.; Fluegel, B.; Mascarenhas, A. Total negative refraction in real crystals for ballistic electrons and light. *Phys. Rev. Lett.* **2003**, *91*, 157404−157407.
(26) Chen, X. L.; He, M.; Du, Y. X.; Wang, W. Y.; Zhang, D. F. Negative refraction, an intrinsic property of uniaxial crystals. *Phys. Rev. B* **2005**, *72*, 113111−113114.
(27) Kang, L.; Zhao, Q.; Li, B.; Zhou, J.; Zhu, H. Experimental verification of a tunable optical negative refraction in nematic liquid crystals. *Appl. Phys. Lett.* **2007**, *90*, 181931−181933.
(28) Pendry, J. B.; Holden, A. J.; Stewart, W. J.; Youngs, I. Extremely low frequency plasmons in metallic mesostrucures. *Phys. Rev. Lett.* **1996**, *76*, 4773−4776.
(29) Pendry, J. B.; Holden, A. J.; Robbins, D. J.; Stewart, W. J. Magnetism from conductors and enhanced nonlinear phenomena. *IEEE Trans. Microwave Theory Tech.* **1999**, *47*, 2075−2084.
(30) Smith, D. R.; Kroll, N. Negative refractive index in left-handed materials. *Phys. Rev. Lett.* **2000**, *85*, 2933−2936.
(31) Schurig, D.; Mock, J. J.; Justice, B. J.; Cummer, S. A.; Pendry, J. B.; Smith, D. R. Metamaterial electromagnetic cloak at microwave frequencies. *Science* **2006**, *314*, 977−980.
(32) Li, J.; Chen, C. T. Double-negative acoustic metamaterial. *Phys. Rev. E* **2004**, *70*, 055602(R).
(33) Chen, H. T.; Padilla, W. J.; Zide, M. O. J.; Gossard, A. C.; Taylor, A. J.; Averitt, R. D. Active terahertz metamaterial devices. *Nature* **2006**, *444*, 597−600.
(34) Landy, N. I.; Sajuyigbe, S.; Mock, J. J.; Smith, D. R.; Padilla, W. J. Perfect metamaterial absorber. *Phys. Rev. Lett.* **2008**, *100*, 207402−207405.
(35) Meng, Q.; Zhang, X.; Cheng, L.; Cao, P.; Li, Y.; Zhang, H.; Wang, G. Deep subwavelength focusing of light by a trumpet hyperlens. *J. Opt.* **2011**, *13*, 075102−075105.
(36) Yao, J.; Tsai, K. T.; Wang, Y.; Liu, Z.; Bartal, G.; Wang, Y. L.; Zhang, X. Imaging visible light using anisotropic metamaterials slab lens. *Opt. Exp.* **2009**, *17*, 22380−22385.
(37) Kruk, S. S.; Powell, D. A.; Minovich, A.; Neshev, D. N.; Kivshar, Y. S. Spatial dispersion of multilayer fishnet metamaterials. *Opt. Express* **2012**, *20*, 15100−15105.
(38) Drachev, V. P.; Podolskiy, V. A.; Kildishev, A. V. Hyperbolic metamaterials: new physics behind a classical problem. *Opt. Express* **2013**, *21*, 15048−15064.
(39) Dresselhaus, M. S.; Dresselhaus, G. Intercalation compounds of graphite. *Adv. Phys.* **2002**, *51*, 1−186.
(40) Jones, M. E.; Marsh, R. E. The preparation and structure of magnesium boride, MgB_2. *J. Am. Chem. Soc.* **1954**, *76*, 1434−1436.
(41) Kunert, J.; Backer, M.; Falter, M.; Schroeder-Obst, D. Comparison of CSD-YBCO growth on different single crystal substrates. *J. Phys. Conf. Ser.* **2008**, *97*, 012148−012152.
(42) Maeno, Y.; Hashimoto, H.; Yoshida, K.; Nishizaki, S.; Fujita, T.; Bednorz, J. G.; Lichtenbrg, F. Superconductivity in a layered perovskite without copper. *Nature* **1994**, *372*, 532−534.
(43) Hu, B.; McCandless, G. T.; Menard, M.; Nascimento, V. B.; Chan, J. Y.; Plummer, E. W.; Jin, R. Surface and bulk structure properties of single crystalline $Sr_3Ru_2O_7$. *Phys. Rev. B* **2010**, *81*, 184104.
(44) Sun, J.; Zhou, J.; Li, B.; Kang, F. Indefinite permittivity and negative refraction in natural material: graphite. *Appl. Phys. Lett.* **2011**, *98*, 101901−101903.
(45) Belashchenko, K. D.; Schilfgaarde, M.; Antropov, V. P. Coexistence of covalent and metallic bonding in the boron intercalation superconductor MgB_2. *Phys. Rev. B* **2001**, *64*, 092503−092506.
(46) Kortus, J.; Mazin, I. I.; Belashchenko, K. D.; Antropov, V. P.; Boyer, L. L. Superconductivity of metallic boron in MgB_2. *Phys. Rev. Lett.* **2001**, *86*, 4656−4659.
(47) Nagamatsu, J.; Nakagawa, N.; Muranaka, T.; Zenitani, Y.; Akimitsu, J. Superconductivity at 39 K in magnesium diboride. *Nature* **2001**, *410*, 63−64.
(48) Guritanu, V.; Kuzmenko, A. B.; Marel, D. V. D. Anisotropic optical conductivity and two colors of MgB_2. *Phys. Rev. B* **2006**, *73*, 104509−104519.
(49) An, J. M.; Pickett, W. E. Superconductivity of MgB_2, covalent bonds driven metallic. *Phys. Rev. Lett.* **2001**, *86*, 4366−4369.
(50) Bednorz, J. G.; Muller, K. A. Possible high Tc superconductivity in the Ba-La-Cu-O system. *Z. Phys. B: Condens. Matter* **1986**, *64*, 189−193.

(51) Wu, M. K.; Ashburn, J. R.; Torng, C. J. Superconductivity at 93 K in a new mixed-phase Y-Ba-Cu-O compound system at ambient pressure. *Phys. Rev. Lett.* **1987**, *58*, 908−910.
(52) Aeppli, G.; Mason, T. E.; Hayden, S. M.; Mook, H. A.; Kulda, J. Nearly singular magnetic fluctuations in the normal state of a high-Tc cuprate. *Science* **1997**, *278*, 1432−1435.
(53) Orenstein, J.; Millis, A. L. Advances in the physics of high-temperature superconductivity. *Science* **2000**, *288*, 468−474.
(54) Lake, B.; Lefmann, K.; Christensen, N. B.; Aeppli, G.; Mcmorrow, D. F.; Ronnow, H. M.; Vorderwisch, P.; Smeibidl, R.; Mangkorntong, N.; Sasagawa, T.; Nohara, M.; Takagi, H. Three-dimensionality of field-induced magnetism in a high-temperature superconductor. *Nat. Mater.* **2005**, *4*, 658−662.
(55) Logvenov, G.; Gozar, A.; Bozovic, I. High-temperature superconductivity in a single copper-oxygen plane. *Science* **2009**, *326*, 699−702.
(56) Moler, K. A. High-temperature superconductivity, how the cuprates hid their stripes. *Nature* **2010**, *468*, 643−644.
(57) Fausti, D.; Tobey, R. I.; Dean, N.; Kaiser, S.; Dienst, A.; Hoffmann, M. C.; Pyon, S.; Takayama, T.; Takagi, H.; Cavalleri, A. Light-induced superconductivity in a stripe-ordered cuprate. *Science* **2011**, *331*, 189−191.
(58) Cava, R. J.; Batlogg, B.; Van Dover, R. B.; Murphy, D. W.; Sunshine, S.; Siegrist, T.; Remeika, J. P.; Rietman, E. A.; Zahurak, S.; Espinosa, G. P. Bulk superconductivity at 91 K in single-phase oxygen-deficient perovskite $YBa_2Cu_3O_{9-\delta}$. *Phys. Rev. Lett.* **1987**, *58*, 1676−1679.
(59) Martin, S.; Fiory, A. T.; Fleming, R. M.; Schneemeyer, L. F.; Waszczak, J. V. Temperature dependence of the resistivity tensor in superconducting $Bi_2Sr_{2.2}$ $Ca_{0.8}Cu_2O_8$ crystals. *Phys. Rev. Lett.* **1988**, *60*, 2194−2197.
(60) Martin, S.; Fiory, A. T.; Fleming, R. M.; Espinosa, G. P.; Cooper, A. S. Anisotropic critical current density in superconducting $Bi_2Sr_2CaCu_2O_8$ crystals. *Appl. Phys. Lett.* **1989**, *54*, 72−74.
(61) Tozer, S. W.; Kleinsasser, A. W.; Penney, T.; Kaiser, D.; Holtzberg, F. Measurement of anisotropic resistivity and Hall constant for single-crystal $YBa_2Cu_3O_{7-x}$. *Phys. Rev. Lett.* **1987**, *59*, 1768−1771.
(62) Pickett, W. E. Electronic structure of the high-temperature oxide superconductors. *Rev. Mod. Phys.* **1989**, *61*, 433−512.
(63) Kim, J. H.; Bozovic, I.; Mitzi, D. B.; Kapitulnik, A.; Harris, J. S, Jr. Optical anisotropy of $Bi_2Sr_2CaCu_2O_8$. *Phys. Rev. B* **1990**, *41*, 7251−7253.
(64) Quijada, M. A.; Tanner, D. B.; Kelley, R. J.; Onellion, M. *a-b* plane anisotropy of single-domain crystals of $Bi_2Sr_2CaCu_2O_8$. *Z. Phys. B* **1994**, *94*, 255−259.
(65) Zibold, A.; Durrler, M.; Geserich, H. P.; Erb, A.; Müller-Vogt, G. Polarized reflectance spectra of a (001) surface of $YBa_2Cu_3O_7$ before and detwinning. *Phys. C* **1990**, *171*, 151−155.
(66) Cooper, S. L.; Nyhus, P.; Reznik, D.; Klein, M. V.; Lee, W. C.; Ginsberg, D. M.; Veal, B. W.; Paulikas, A. P.; Dabrowski, B. Interbilayer charge dynamics in $YBa_2Cu_3O_{6+x}$. *Phys. Rev. Lett.* **1993**, *70*, 1533−1536.
(67) Nee, T. Anisotropic optical properties of $YBa_2Cu_3O_7$. *J. Appl. Phys.* **1992**, *71*, 6002−6007.
(68) Koch, B.; Geserich, H. P.; Wolf, T. Anisotropy of the reflectance spectrum and of the dielectric function of $YBa_2Cu_3O_7$ within the (001) plane. *Solid State Commun.* **1989**, *71*, 495−499.
(69) Zelezny, V.; Tanner, D. B.; Kamaras, K.; Kozeeva, L. P.; Pavlyuk, A. A. Anisotropic optical properties of single-crystal $GdBa_2Cu_3O_{7-\delta}$. *Z. Phys. B* **1995**, *96*, 313−318.
(70) Ibach, H.; Lüth, H. *Solid-State Physics*; Springer: Berlin, 2003; pp 292−294.
(71) Cooper, S. L.; Reznik, D.; Kotz, A.; Karlow, M. A.; Liu, R.; Klein, M. V. Optical studies of the *a-*, *b-*, and *c*-axis charge dynamics in $YBa_2Cu_3O_{6+x}$. *Phys. Rev. B* **1993**, *47*, 8233−8248.
(72) Collins, R. T.; Schlesinger, Z.; Chandrashekhar, G. V.; Shafer, M. W. Infrared study of anisotropy in single-crystal $La_{2-x}Sr_xCuO_4$. *Phys. Rev. B* **1989**, *39*, 2251−2254.
(73) Ruddlesden, S. N.; Popper, P. The compound $Sr_3Ti_2O_7$ and its structure. *Acta Crystallogr.* **1958**, *11*, 54−55.
(74) Maeno, Y.; Hashimoto, H.; Yoshida, K.; Nishizaki, S.; Fugita, T.; Bednorz, J. G.; Lichtenberg, F. Superconductivity in a layered perovskite without copper. *Nature* **1994**, *372*, 532−534.
(75) Lichtenberg, F. The story of Sr_2RuO_4. *Prog. Solid State Chem.* **2002**, *30*, 103−131.
(76) Huang, Q.; Lynn, J. W.; Erwin, R. W.; Jarupatrakorn, J.; Cava, R. J. Oxygen displacements and search for magnetic order in $Sr_3Ru_2O_7$. *Phys. Rev. B* **1998**, *58*, 8515−8521.
(77) Klein, L.; Dodge, J. S.; Ahn, C. H.; Snyder, G. J.; Geballe, T. H.; Beasley, M. R.; Kapitulnik, A. Anomalous spin scattering effects in the badly metallic itinerant ferromagnet $SrRuO_3$. *Phys. Rev. Lett.* **1996**, *77*, 2774−2777.
(78) Katsufuji, T.; Kasai, M.; Tokura, Y. In-plane and out-of-plane optical spectra of Sr_2RuO_4. *Phys. Rev. Lett.* **1996**, *76*, 126−129.
(79) Mirri, C.; Baldassarre, L.; Lupi, S.; Ortolani, M.; Fittipaldi, R.; Wecchione, A.; Calvani, P. Anisotropic optical conductivity of $Sr_3Ru_2O_7$. *Phys. Rev. B* **2008**, *78*, 155132−155137.
(80) Johnson, L. G. Optical properties of graphite. *Phys. Rev. B* **1973**, *7*, 2275−2285.
(81) Taft, E. A.; Philipp, H. R. Optical properties of graphite. *Phys. Rev.* **1965**, *138*, A197−A202.
(82) Djurisic, A. B.; Li, E. H. Optical properties of graphite. *J. Appl. Phys.* **1999**, *85*, 7404−7410.
(83) Greenaway, D. L.; Harbeke, G. Anisotropy of the optical constants and the band structure of graphite. *Phys. Rev.* **1969**, *178*, 1340−1348.
(84) Palik, E. D. *Handbook of Optical Constants of Solids II*; Academic Press: London, 1991; pp 449−460.
(85) Alekseyev, L.; Podolskiy, V. A.; Narimanov, E. Homogeneous hyperbolic systems for terahertz and far-infrared frequencies. *Adv. Optoelectron.* **2012**, *2012*, 267564.
(86) Wang, R.; Sun, J. B.; Zhou, J. Indefinite permittivity in uniaxial single crystal at infrared frequency. *Appl. Phys. Lett.* **2010**, *97*, 031912−031914.
(87) Vella-coleiro, G. P.; Smith, D. H.; Van Uitert, L. G. Resonant motion of domain walls in yttrium gadolinium iron garnets. *J. Appl. Phys.* **1972**, *43*, 2428−2430.
(88) Dionne, G. F. Magnetic relaxation and anisotropy effects on high-frequency permeability. *IEEE Trans. Magn.* **2003**, *39*, 3121−3126.
(89) Li, T.; Patz, A.; Mouchliadis, L.; Yan, J.; Lograsso, T. A.; Perakis, I. E.; Wang, J. Femtosecond switching of magnetism via strongly correlated spin-charge quantum excitations. *Nature* **2013**, *496*, 69−73.
(90) Pendry, J. B. A chiral route to negative refraction. *Science* **2004**, *306*, 1353−1355.
(91) Zhang, S.; Park, Y. S.; Li, J.; Lu, X.; Zhang, W.; Zhang, X. Negative refraction index in chiral metamaterials. *Phys. Rev. Lett.* **2009**, *102*, 023901.
(92) Ginis, V.; Tassin, P.; Soukoulis, C. M.; Veretennicoff, I. Enhancing optical gradient forces with metamaterials. *Phys. Rev. Lett.* **2013**, *110*, 057401.